Article

Not peer-reviewed version

A New Approach to the Preparation of Stable Oxide-Composite Cobalt-Samarium Catalysts for the Production of Hydrogen by Dry Re-Forming of Methane

Alexey S. Loktev *, Alexey G. Dedov, Veronika A. Arkhipova, Mikhail A. Bykov, Alexey A. Sadovnikov, Kirill A. Cherednichenko, Georgy A. Shandryuk

Posted Date: 5 July 2023

doi: 10.20944/preprints202307.0337.v1

Keywords: heterogeneous catalysis; hydrogen; synthesis gas; dry reforming of methane; cobalt-samarium oxide catalysts

Article

A NEW APPROACH TO THE PREPARATION OF STABLE OXIDE-COMPOSITE COBALT-SAMARIUM CATALYSTS FOR THE PRODUCTION OF HYDROGEN BY DRY REFORMING OF METHANE

A. G. Dedov [1,2], A. S. Loktev [1,2,*], V. A. Arkhipova [2], M. A. Bykov [3], A. A. Sadovnikov [1], K. A. Cherednichenko [2] and G. A. Shandryuk [1]

[1] A. V. Topchiev Institute of Petrochemical Synthesis, Russian Academy of Sciences, Leninsky Prosp. 29, 119991 Moscow, Russia
[2] National University of Oil and Gas «Gubkin University», Leninsky Prosp. 65, 119991 Moscow, Russia
[3] Department of Chemistry, Lomonosov Moscow State University, Leninskie gory 3/1, 119991, Moscow, Russia
* Correspondence: al57@rambler.ru, genchem@gubkin.ru

Abstract: A new approach to preparing a series of Co/Sm_2O_3 catalysts for hydrogen production by dry reforming of methane (DRM) is developed. The catalysts precursors are synthesized by a simple method, including evaporation of aqueous solutions of cobalt and samarium nitrates, followed by a short-term calcination of the resulting material. The as-prepared and spent catalysts are characterized using X-ray diffraction (XRD), scanning electron microscopy (SEM), transmission electron microscopy (TEM), temperature-programmed reduction (H_2-TPR), and thermogravimetric analysis (TGA). It is shown that the content of cobalt in the synthesized materials affects their phase composition and carbonization resistance in the DRM reaction. It is demonstrated that preheating under N_2 affords catalysts providing stable hydrogen and CO yields of 94-98 % for at least 50 h at 900°C. These yields are among the highest ones currently available for DRM catalysts derived from Co-Sm complex oxides. It is found that reduction in the amount of cobalt in the catalyst and its preheating to an operating temperature of 900°C in a nitrogen flow contribute to preventing catalyst carbonization and metal particles sintering.

Keywords: heterogeneous catalysis; hydrogen; synthesis gas; dry reforming of methane; cobalt-samarium oxide catalysts

1. Introduction

The increasing threat of global climate change has prompted the governments of 195 countries to adopt the "Paris Agreement" that aims to reduce greenhouse gas emissions, primarily by decarbonizing the economy [1,2]. In this regard, hydrogen is considered the most environmentally friendly alternative fuel, since its use as a fuel is accompanied only by the release of water vapor into the air. Hydrogen has the highest energy intensity per unit mass but low density. In addition to being a promising fuel, hydrogen is used in increasing volumes in the processes of ammonia synthesis and oil refining and as a synthesis gas component for the production of methanol and a number of petrochemicals [1–4].

The main industrial process of hydrogen production is the steam reforming of methane (1), which a high-energy endothermic process requiring the production of considerable volumes of water vapor [2,5,6].

$$CH_4+H_2O \rightleftharpoons CO+3H_2 \quad \Delta H^0_{298}= +206 \text{ kJ} \qquad (1)$$

Promising processes for hydrogen production from methane are partial oxidation of methane, POM, (2) and dry reforming of methane, DRM, (3).

$$2CH_4 + O_2 \rightleftharpoons 2CO + 4H_2 \quad \Delta H^0_{298}= -36 \text{ kJ} \qquad (2)$$

Preprints (www.preprints.org) | NOT PEER-REVIEWED | Posted: 5 July 2023 doi:10.20944/preprints202307.0337.v1

$$CH_4 + CO_2 \rightleftharpoons 2CO + 2H_2 \quad \Delta H^0_{298} = +247 \text{ kJ} \qquad (3)$$

Since reaction (2) is exothermic, the POM process in combination with the steam reforming of methane is implemented in the autothermal mode. In addition, POM allows the production of synthesis gas (H_2: CO = 2:1) suitable for direct processing into petrochemical products [5–8]. The practical application of POM is largely limited by the need to use pure oxygen, the related explosion hazard, and the possible sintering of metal active centers in the event of "hot spots" in the catalyst layer.

The process of hydrogen production by the DRM reaction has been most extensively studied in recent decades. For example, the number of publications on this topic in 1990-2022 exceeded 1000, including 863 scientific articles with the citation number above 6, and 34 reviews [9]. The explosive interest in this topic is due to a number of factors. Firstly, these are the above-mentioned efforts of most countries to reduce the greenhouse effect [1–3]. The DRM process allows the utilization of methane and carbon dioxide, which are the main greenhouse gases. Secondly, the DRM process is a way to produce hydrogen and other valuable products by processing of renewable raw materials, biogas, one of the promising decarbonization strategies [10]. Thirdly, the industrial process of hydrogen production by the steam reforming of methane includes an additional stage of the steam reforming of CO (4):

$$CO + H_2O \rightleftharpoons CO_2 + H_2 \qquad (4)$$

CO_2 generated by this process must also be disposed of.

In addition, the joint methane steam reforming and DRM can also be used for the utilization of CO_2 captured from the flue gases of methane steam reforming plants [2]. Finally, the DRM process renders it possible to produce synthesis gas, which is a suitable intermediate for the synthesis of dimethyl ether, Fischer-Tropsch synthesis of hydrocarbons etc. [1–4,6,9,11–16]. Furthermore, the synthesis gas of the DRM process can be used in fuel cells [13].

As for the use of the DRM process is practice, this process is realized mostly on a pilot scale and in combination with the steam reforming of methane in order to control the composition of the resulting synthesis gas [15–18]. The CALCOR process is known [15–17,19]; however, it is aimed at obtaining primarily carbon monoxide (H_2:CO = 0.42:1) and, therefore, is accomplished at a large excess of CO_2. The industrial implementation of DRM is constrained by a number of features of this process, such as high endothermicity associated with the stability of CO_2 and CH_4 molecules and a significant formation of coke deposits and "sintering" of active catalyst centers associated with a high temperature of the process. A high temperature of the process also requires complex hardware design. In addition, it was shown that the DRM process conducted at elevated pressures is accompanied by an enhanced carbonization of catalysts. Therefore, the synthesis gas produced by DRM and intended for subsequent processing will require a costly stage of its compression [1,13,15,17,20–22].

According to thermodynamic calculations, at fairly low temperatures DRM does not allow a high yield of synthesis gas. To achieve high yields of synthesis gas (H_2 : CO = 1 : 1) by reaction (3) with the reagents conversion close to 100% and reduced carbon formation by the methane pyrolysis reaction (5), a ratio of CO_2 : CH_4 = 1 : 1, a temperature above 850°C, and atmospheric pressure are required [12,13,16,17,22–25].

$$CH_4 \rightleftharpoons C + 2H_2 \quad \Delta G^0_{298} \le 0 \text{ at } T \ge 658 \text{ C.} \qquad (5)$$

These conditions also contribute to the reverse water gas shift reaction (6) that affects the ratio of DRM products and the value of CO_2 conversion:

$$CO_2 + H_2 \rightleftharpoons CO + H_2O \quad \Delta G^0_{298} \le 0 \text{ at } T \ge 700 \text{ C.} \qquad (6)$$

Carbon formation in the DRM process is possible not only by reaction (5) but also by the disproportionation of CO (7) and the hydrogenation of CO (8) and CO_2 (9) [12,26].

$$2CO \rightleftharpoons C + CO_2 \quad \Delta H^0_{298} = -172 \text{ kJ} \qquad (7)$$

$$CO + H_2 \rightleftharpoons C + H_2O \quad \Delta H^0_{298} = -131 \text{ kJ} \qquad (8)$$

$$CO_2 + 2H_2 \rightleftharpoons C + 2H_2O \quad \Delta H^0_{298} = -90 \text{ kJ} \qquad (9)$$

However, these reactions are exothermic, thermodynamically unfavorable at high temperatures, and probably proceed in the opposite direction.

 doi:10.20944/preprints202307.0337.v1

One of the key approaches to the practical implementation of the DRM process considered in most relevant publications is to design selective, stable, and carbonization resistant catalysts. Objectives are to prevent sintering of the active centers of catalysts and formation of stable forms of surface carbon (graphite, carbon fibers, and nanotubes), which deactivate active centers, destroy the catalyst, and block the passage of gases through a reactor. Complex oxides of the perovskite structure are in most common use as promising DRM catalysts [1–3,5,6,10–15]. As a result of pre-reduction or contact with reagents perovskite structure catalysts are transformed into composites containing a metal phase highly dispersed in an oxide matrix, which in some cases enables one to achieve high activity, selectivity, and stability in DRM. Among these compounds, there are catalysts based on nickelates and cobalates of rare earth elements [5,11,27–33]. According to these studies, perovskite precursors of catalysts can be synthesized by various methods, such as solid-phase synthesis, self-propagating high-temperature synthesis, sol-gel synthesis, decomposition of specially synthesized complex compounds, etc. The choice of the synthesis method largely determines the properties of the DRM catalysts.

Previously, we synthesized and tested in DRM lanthanum nickelate [30] and samarium cobaltate [29] perovskite structures obtained by the thermal decomposition of specially synthesized heterometallic complex compounds $(M^1(phen)x][M^2(NO_3)_y(H_2O)]\cdot zMeCN$, where M^1 is Ni or Co, M^2 is La or Sm, phen is o-phenanthroline, and MeCN is methyl acetate). These compounds served as precursors of efficient DRM catalysts, composites containing metallic nickel or cobalt dispersed in a matrix of lanthanum or samarium oxides. However, during the DRM process, despite the thermodynamically favorable conditions of the process, their surface was subjected to significant carbonization which resulted in blocking of the gas flow in the reactor. Using a complex procedure for the supercritical antisolvent deposition of a complex compound--the precursor of perovskite $SmCoO_3$, the catalyst particle size was reduced and catalyst carbonization was avoided [29].

However, we have shown that the production of efficient DRM catalysts does not require the mandatory synthesis of a completely single-phase initial perovskite [34,35]. Composites containing, along with the perovskite phase, the phases of nickel, cobalt, and rare earth elements oxides can be synthesized using a simple evaporation of aqueous solutions of nickel, cobalt and rare earth elements (REE) salts. In the DRM process, these composites form catalysts consisting of metallic nickel or cobalt dispersed in an REE oxide. These catalysts make it possible to obtain synthesis gas with a yield above 90% but undergo significant carbonization.

In order to create a DRM catalyst less susceptible to carburization, we synthesized an oxide composite containing 2 wt. % cobalt. This material was prepared by the simple evaporation of an aqueous solution of cobalt and samarium nitrates, followed by calcination of the resulting material at 700°C [36]. It was assumed that due to a decrease in the cobalt content in this material compared to the $SmCoO_3$ perovskite containing 23 wt. % cobalt metallic cobalt particles more resistant to sintering and subsequent carbonization would be obtained. It is known that the deposition of perovskite systems on various substrates often increases their efficiency in DRM catalysis [11,14,16,20]. It was supposed that the synthesized material would contain samarium cobaltate $SmCoO_3$ dispersed in a matrix of samarium oxide. However, the formed composite consisted of samarium oxide and samarium cobaltite, Sm_2CoO_4, which apparently resulted from the interaction of $SmCoO_3$ with an excess of samarium oxide.

It was found that this material after prereduction in CH_4 and CO_2 mixture or in hydrogen flow formed catalyst which demonstrated low efficiency in DRM. And only after a long-term exposure in the CH_4/CO_2 flow showed synthesis gas yields of 88-90 % at 900°C.

The aim of the present study is to find optimal conditions for the preparation of highly efficient stable and carbonization resistant Co/Sm_2O_3 catalysts with various cobalt content for hydrogen production by DRM.

2. Materials and Methods

2.1. Materials

We used the following commercial Sigma-Aldrich reagents: $Co(NO_3)_2 \cdot 6H_2O$ CAS 10026-22-9, and $Sm(NO_3)_3 \cdot 6H_2O$ CAS 13759-83-6.

2.2. Preparation of Catalyst

The designations of the synthesized materials--catalysts precursors--and the amounts of reagents used for their synthesis are given in Table 1. The amounts of reagents corresponded to the cobalt content in the resulting catalyst (Table 1). The $Co(NO_3)_2 \bullet 6H_2O$ and $Sm(NO_3)_3 \bullet 6H_2O$ samples were dissolved in 30 ml of distilled water under stirring in a glass beaker. The obtained solutions were heated under stirring until water evaporation. The resulting mass was transferred into an alundum crucible and heated in a Nabertherm muffle furnace for 3 h at 300°C. The solid product was crushed, heated in the muffle furnace for 2.5 h to 800°C, and kept for 2 h at this temperature.

Table 1. The code of catalysts, the mass of reagents taken for the synthesis of catalysts and the specific surface area (S_{BET}) of the materials obtained.

Code of catalysts	Mass of $Co(NO_3)_2 \bullet 6H_2O$, g	Mass of $Sm(NO_3)_3 \bullet 6H_2O$, g	S_{BET}, m^2/g
2%Co/Sm_2O_3	0.49	12.49	1.79
5%Co/Sm_2O_3	1.23	12.11	2.82
10%Co/Sm_2O_3	2.47	11.47	3.45
23%Co/Sm_2O_3	2.91	4.47	3.82

2.3. Characterization

The specific surface area S_{BET} of the samples was measured by the method of low-temperature nitrogen adsorption on an ATKh-06 analyzer (Katakon, Russia). The samples were degassed in a nitrogen flow (1 atm) at 200°C for an hour prior to analysis. Based on the data obtained, the specific surface area of the samples was calculated using the Brunauer–Emmett–Teller (BET) model and the five-points method in the partial pressure range of 0.05–0.25 P/P_0.

The powder X-ray diffraction study (XRD) of freshly prepared and spent catalysts was carried out on a Rigaku MiniFlex 600 diffractometer (CuKα radiation, detector with graphite monochromator, and Cu anticathode). The XRD data were processed using the database of the International Center for Diffraction Data (ICDD).

Thermogravimetric analysis (TGA) was performed on a TGA/DSC 3+ simultaneous thermal analyzer (Mettler Toledo) in an air flow in the range of 30–1000°C at a heating rate of 10°C/min. The TGA data were processed using the STARe Excellence software.

The micromorphology of all samples was studied by scanning electron microscopy (SEM) on a Carl Zeiss NVision 40 high-resolution microscope equipped with an Oxford Instruments X-MAX detector (80 mm^2) and operating at an accelerating voltage of 1-20 kV. SEM images were taken in InLens (SE2) and ESB modes with an Everhart-Thornley detector at accelerating voltages of 1 and 7 kV.

The microstructure and elemental mapping of some spent catalysts were investigated on a TJEOL JEM-2100 UHR transmission electron microscope (TEM) operating at an accelerating voltage of 200 kV. Sample powders were dispersed in ethanol and dropped onto a TEM cooper grid (Ted Pella, Inc.). TEM micrographs were collected in the bright-field mode using an Olympus Quemesa 11-megapixel CCD camera. The dark-field sample images and elemental mapping were performed in the STEM mode.

The temperature-programmed reduction (H_2-TPR) was performed in a flow quartz reactor with an inner diameter of 2 mm at a heating rate of 7.5°C/min. Temperature was measured with the aid of a chromel-alumel thermocouple (K-type). The H_2/Ar flow (5 vol. % H_2) velocity was 50 ml/min. The

Preprints (www.preprints.org) | NOT PEER-REVIEWED | Posted: 5 July 2023 doi:10.20944/preprints202307.0337.v1

H_2 content in the outlet gas flow was assessed on a Krystallyuks-4000M chromatograph equipped a thermal conductivity detector.

In addition, the H_2-TPR of the catalysts was carried out in the same mode on an USGA-101/M3 chemisorption analyzer (LLC UNISIT, Russia).

2.4. Catalytic Experiments

The catalytic performance of 2%Co/Sm_2O_3, 5%Co/Sm_2O_3, 10%Co/Sm_2O_3, 23%Co/Sm_2O_3 materials in the DRM process was tested at atmospheric pressure in a fixed bed flow quartz reactor (inner diameter 18 mm) with an axial pocket for thermocouple (outer diameter 8 mm). The tip of the thermocouple (chromel-alumel (K)) was positioned in the center of the catalyst layer. Powdered catalysts precursors were pressed into pellets, grinded, and a fraction with 0.5-1 mm grains was used in further experiments. The catalyst precursor (0.2 g, layer height 1 mm) was placed on a quartz fiber substrate. The catalyst precursor was heated to 900 °C in a nitrogen stream (JSC NIIKM, Russia, nitrogen content 99.999%). When the catalyst was heated in the nitrogen flow, after its supply was stopped, a gas mixture of CH_4 and CO_2 (JSC "Moscow Gas Processing Plant", Russia, purity at least 99.9%) was fed into the reactor. The ratio of CH_4 : CO_2 was 1, and the feed rate of the nitrogen or gas mixture was 15 L × g^{-1} × h^{-1}. The gas velocity at the reactor inlet and outlet was measured with a foam flow meter. The temperature change in the reactor was carried out using a programmable temperature controller. The products were analyzed at a fixed temperature, and the temperature was adjusted to other set values without stopping the supply of reagents.

The composition of gaseous products was analyzed online by GLC on GALS 311 chromatographs equipped with thermal conductivity detectors using He as a carrier gas. The concentrations of H_2, CH_4, and CO were estimated at 30°C in a 2 m × 3 mm steel column packed with NaX zeolite. The H_2 concentration was calculated using a special calibration graph. To detect CH_4, CO_2, ethylene, and ethane a similar column filled by a Porapak Q at 70°C was used. The admixtures of C_{2+} hydrocarbons were determined at 70°C using a similar column filled by 5% Na_2CO_3 on alumina. The chromatographic data were analyzed using the EKOCHROM software (SKB of the Zelinsky Institute of Organic Chemistry, Russian Academy of Sciences). All chromatograms were calculated by internal normalization with correction made for the molecular weights of the components.

2.4.1. Calculations

Methane conversion, X(CH_4), was calculated as

$$X(CH_4) = \frac{W_{in}(CH_4) - W_{out}(CH_4)}{W_{in}(CH_4)} \times 100\%,$$

where $W_{in}(CH_4)$ is the quantity (mol) of CH_4 injected in the reactor and $W_{out}(CH_4)$ is the quantity (mol) of CH_4 at the reactor outlet.

CO_2 conversion X(CO_2) were calculated similarly.

Hydrogen yield, Y(H_2), was calculated as

$$Y(H_2) = \frac{W_{out}(H_2)}{2W_{in}(CH_4)} \times 100\%,$$

where $W_{out}(H_2)$ is quantity (mol) of H_2 at the reactor outlet and $W_{in}(CH_4)$ is the quantity (mol) of CH_4 injected in the reactor.

CO yield, Y(CO), was calculated as:

$$Y(CO) = \frac{W_{out}(CO)}{W_{in}(CH_4) + W_{in}(CO_2)} \times 100\%,$$

where $W_{out}(CO)$ is the quantity (mol) of CO at the reactor outlet and $W_{in}(CH_4)$ and $W_{in}(CO_2)$ are, accordingly, the quantities (mol) of CH_4 and CO_2 injected in the reactor.

Preprints (www.preprints.org) | NOT PEER-REVIEWED | Posted: 5 July 2023 doi:10.20944/preprints202307.0337.v1

3. Results and Discussion

In specially blank experiments conducted in the reactor without a catalyst, a slight carbonization of reactor walls was detected mainly after a layer of quartz nozzle and quartz fiber. At the same time, the trace amounts of CO and hydrogen were recorded in exhaust gases along with unreacted reagents.

3.1. Characterization of freshly prepared materials

According to the XRD data, the synthesized sample of 2%Co/Sm_2O_3 contains phases Sm_2O_3 (ICDD 96-101-0341, 88 wt. %) and Sm_2CoO_4 (ICDD 96-200-2267, 12 wt. %) (Figure 1a). The phase content was calculated by the Rietveld method [37].

Sample 5%Co/ Sm_2O_3 (Figure 1b), along with Sm_2O_3 (ICDD 96-101-0341, 86 wt. %), contains the $SmCoO_3$ phase (ICDD 96-412-4856, 14 wt. %).

Sample 10%Co/ Sm_2O_3 (Figure 1c), along with Sm_2O_3 (ICDD 99-208-1967, 47 wt. %), contains $SmCoO_3$ (ICDD 99-204-5928, 53 wt. %).

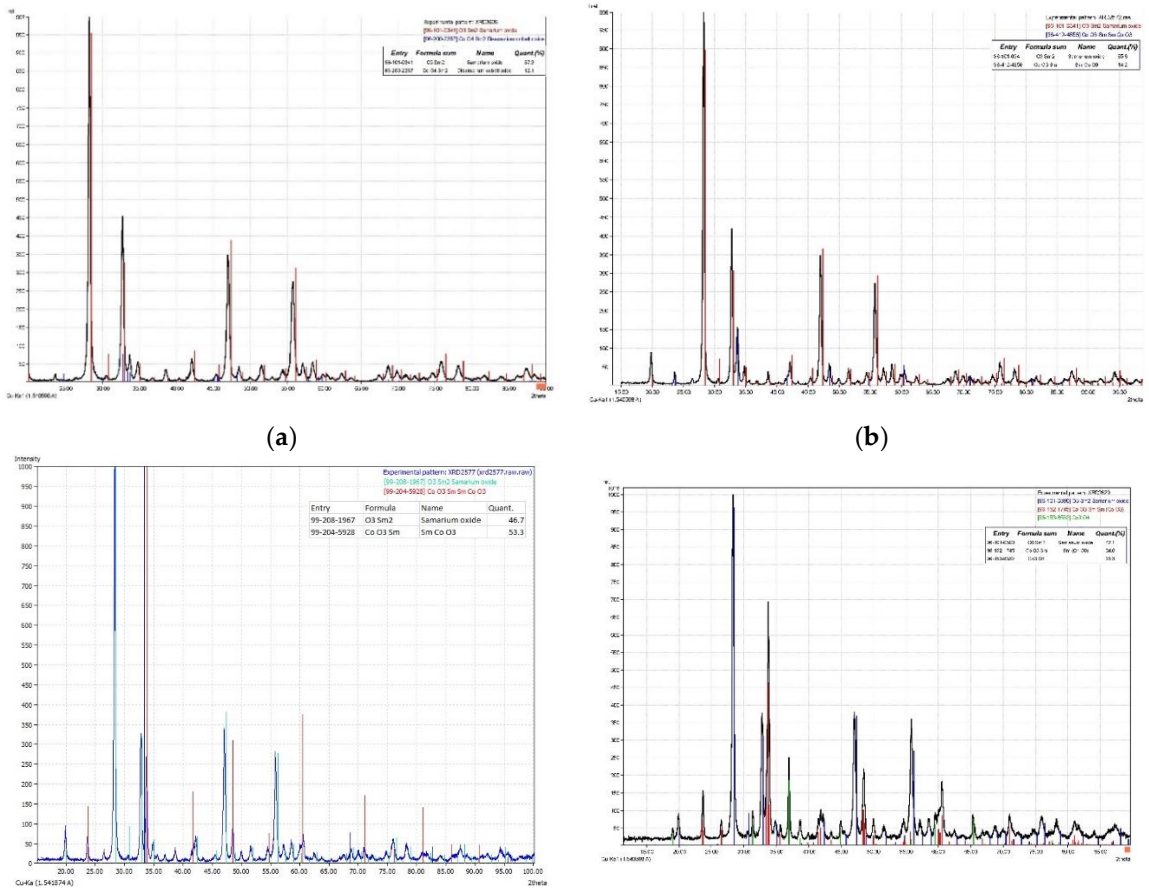

Figure 1. XRD patterns of (**a**) 2%Co/Sm_2O_3, (**b**) 5%Co/Sm_2O_3, (**c**) 10%Co/Sm_2O_3, and (**d**) 23%Co/Sm_2O_3.

Sample 23%Co/ Sm_2O_3 (Figure 1d), in which the amount of cobalt corresponds to its content in the $SmCoO_3$ perovskite, according to XRD data, contains only 35 wt. % of $SmCoO_3$ (ICDD 96-152-1745), as well as Sm_2O_3 (ICDD 96-101-0590, 42 wt. %) and Co_3O_4 (ICDD 96-153-8532, 23 wt. %). Thus, the samarium/cobalt ratio in the synthesized complex oxides significantly affects their phase composition.

The SEM images of the synthesized materials (Figure 2 a-d) show that the 2%Co/Sm_2O_3 sample (Figure 2a) is formed by flat particles with an undeveloped porous structure, which corresponds to a low specific surface area of the sample (Table 1).

Preprints (www.preprints.org) | NOT PEER-REVIEWED | Posted: 5 July 2023 doi:10.20944/preprints202307.0337.v1

In the images of 5%Co/Sm_2O_3 (Figure 2b) and 23%Co/Sm_2O_3 (Figure 2d) samples taken at a higher resolution, particles of a similar shape are seen; their lateral faces contain mesopores with a diameter of about 20 nm.

The 10%Co/Sm_2O_3, (Figure 2b) sample also contains flat particles with the undeveloped porous structure.

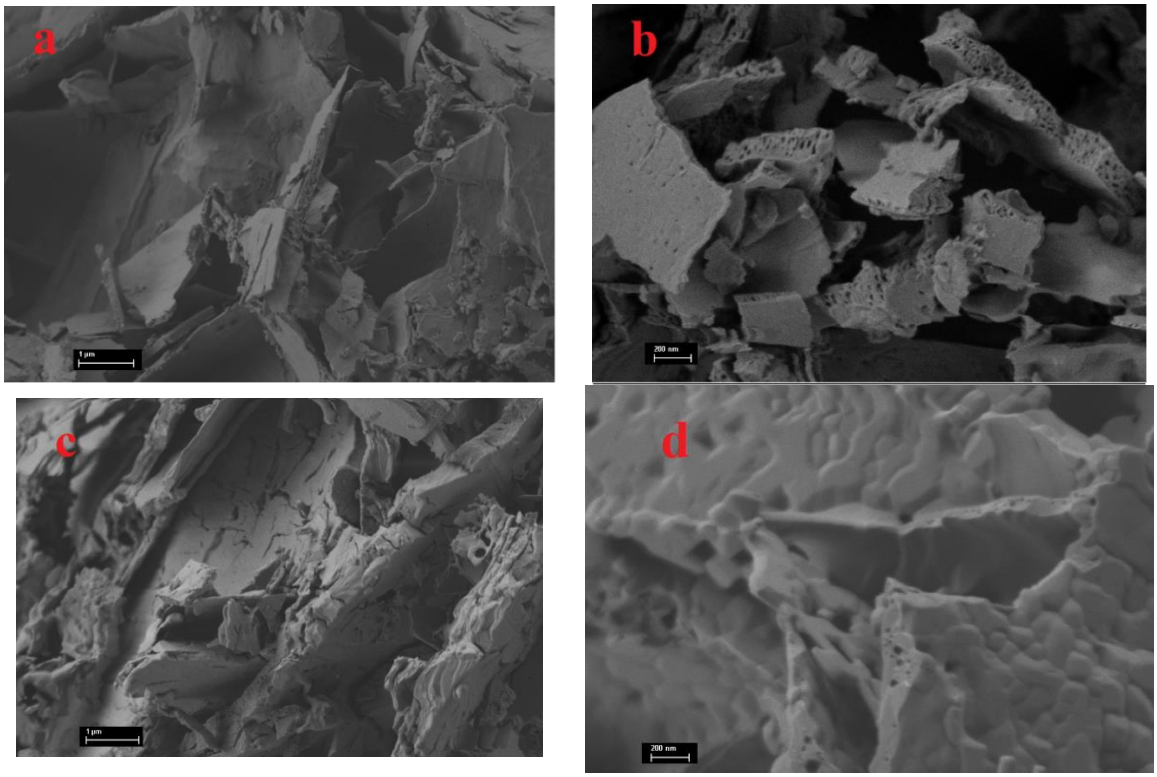

Figure 2. SEM images of (**a**) 2%Co/Sm_2O_3, (**b**) 5%Co/Sm_2O_3, (**c**) 10%Co/Sm_2O_3, and (**d**) 23%Co/Sm_2O_3.

The H_2-TPR profile of 2%Co/Sm2O3 (Figure 3a) reveals the presence of three regions of hydrogen absorption. Less intense peaks with maxima at 310 and 400°C are probably related to reduction of a small amount of Co_3O_4 contained in the catalyst [38], which was not recorded by XRD. An intense peak with a maximum at 540°C, according to [11,31,39], can be assigned to the reduction of samarium cobaltite by reaction (10):

$$Sm_2CoO_4 + H_2 = Sm_2O_3 + Co + H_2O. \quad (10)$$

The H_2-TPR profile of 5%Co/Sm_2O_3 (Figure 3b) exhibits a low-intensity peak with maxima at 420°C and an intense peak with a maximum at 530 °C, which, according to [11,31,39], can be attributed to the staged reduction of samarium cobaltate by reactions (11) and (12):

$$2SmCoO_3 + H_2 = 2SmCoO_{2,5} + H_2O \quad (11)$$

$$2SmCoO_{2,5} + 2H_2 = Sm_2O_3 + 2Co + 2H_2O \quad (12)$$

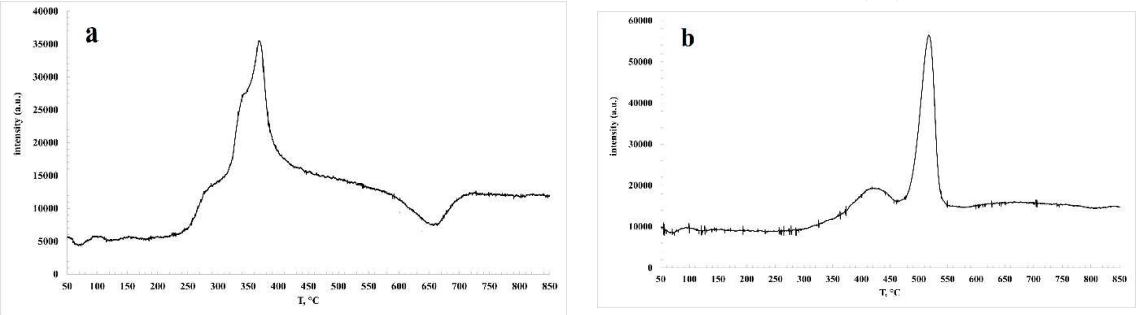

Preprints (www.preprints.org) | NOT PEER-REVIEWED | Posted: 5 July 2023 doi:10.20944/preprints202307.0337.v1

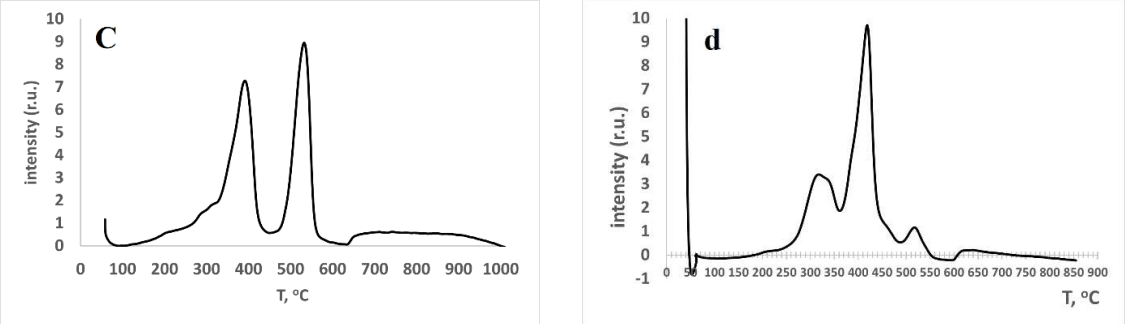

Figure 3. H_2-TPR profiles of (**a**) 2%Co/Sm_2O_3, (**b**) 5%Co/Sm_2O_3, (**c**) 10%Co/Sm_2O_3, and (**d**) 23%Co/Sm_2O_3.

The H_2-TPR profiles of 10%Co/Sm_2O_3 (Figure 3c) and 23%Co/Sm_2O_3 (Figure 3d) are recorded by the USGA analyzer. The H_2-TPR profile of 10%Co/Sm_2O_3 shows two intense peaks with maxima at 390 and 532°C, which, according to [11,31,39], can also be attributed to the staged reduction of samarium cobaltate by reactions (11) and (12).

The H_2-TPR graph of 23%Co/ Sm_2O_3 exhibits a peak with a maximum at 318°C corresponding to the reduction of cobalt oxides and an intense peak with a maximum at 419°C, which can be assigned to the reduction of both cobalt oxides and samarium cobaltate by reaction (11). A less intense peak with a maximum at 517°C probably corresponds to reaction (12). In general, the H_2-TPR data obtained for the synthesized samples are consistent with the XRD analysis (Figure 1 and comments).

3.2. Results of Catalytic Experiments

As indicated in our previous paper [36], it takes a long time for the 2%Co/Sm_2O_3 catalyst preheated to 900°C in the flow of CH_4/CO_2 (1 : 1) or hydrogen flow to reach the optimal operating mode. In the present work, 2%Co/Sm_2O_3 was preheated to 900 °C for an hour in a high-purity nitrogen flow. The results are shown in Figure 4.

It can be seen that in contrast to [36] results, immediately after the mixture of CH_4 and CO_2 was fed to the reactor, the yield of the synthesis gas (CO : H_2 = 1 : 1) equal to 96 was achieved. The conversion of CH_4 was 97%, and the conversion of CO_2 was 99%. In a long-term experiment with intermediate cooling and reheating to 900°C in the high-purity nitrogen, the stable performance of the catalyst for 50 h was observed. The values of CO_2 conversion and CO yield higher than the values of methane conversion and hydrogen yield are apparently due to an insignificant reverse water gas shift reaction (6) along with the DRM reaction (3). Since, in accordance with [36], in the case of the 2%Co/Sm_2O_3 catalyst, a decrease in temperature leads to a decrease in the conversion of reagents and the yields of products, this catalyst was not tested at temperatures less than 900°C. Our results demonstrate that a highly efficient and stable DRM catalyst is formed *in situ* immediately after the contact of 2%Co/Sm_2O_3 preheated to 900 °C in N_2 flow with the CH_4-CO_2. mixture.

Preprints (www.preprints.org) | NOT PEER-REVIEWED | Posted: 5 July 2023 doi:10.20944/preprints202307.0337.v1

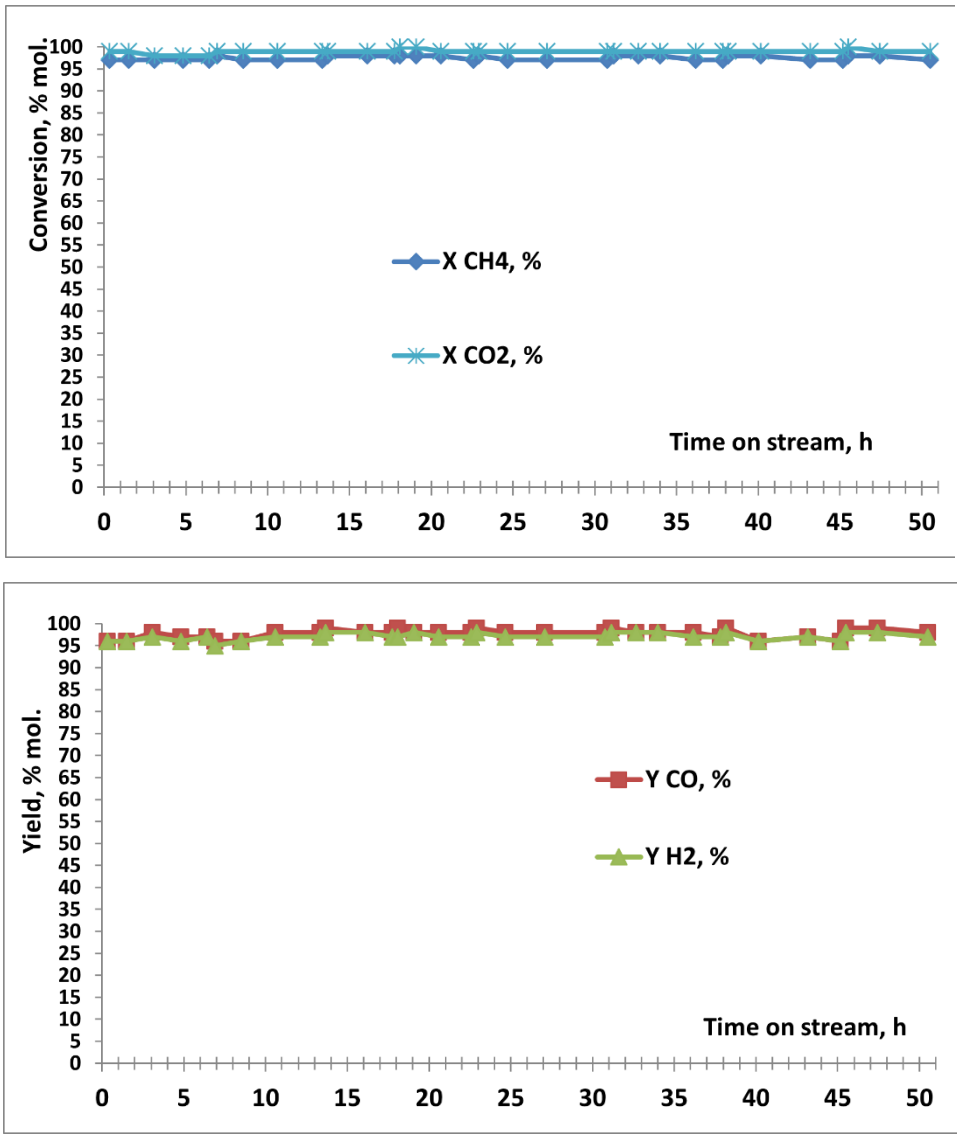

Figure 4. The performance in DRM process on 2%Co/Sm_2O_3 derived catalyst preheated to 900°C in N_2 flow.

The 5%Co/Sm_2O_3 and 10%Co/Sm_2O_3 samples, which were also preheated to 900°C for an hour in the high-purity nitrogen flow, as well as the 2%Co/Sm_2O_3 sample, also immediately formed catalysts which showed high yields of CO and H_2 (Figures 5, 6).

The data in Figure 5 indicate that for the catalyst derived from 5%Co/Sm_2O_3 the CH_4 conversion is 95-98%, the CO_2 conversion is 100%, the CO yield is 97-98%, and the H_2 yield is 95-97%. When temperature was reduced to 800°C, the CH_4 conversion decreased to 83-84%, the CO_2 conversion decreased to 90-91%, the CO yield decreased to 81-83%, and the H_2 yield decreased to 82%. At 700°C, the CH_4 conversion was 46-47%, the CO_2 conversion was 58-59%, the CO yield was 47-49%, and the H_2 yield was 39-41%, while at 600°C almost no DRM was observed. A subsequent increase in temperature to 900°C restored the activity of the catalyst. When the experiment was continued up to 50 h, high values of CH_4 conversion (94-96%), CO_2 conversion (99-100%), CO yield (94-97%), and H_2 yield (94-96%) were maintained. The observed values of CO_2 conversion and CO yield higher than those of methane conversion and hydrogen yield also indicate that, along with the DRM reaction (3), an insignificant reverse water gas shift reaction (6) occurs and its contribution increases with decreasing temperature.

Preprints (www.preprints.org) | NOT PEER-REVIEWED | Posted: 5 July 2023 doi:10.20944/preprints202307.0337.v1

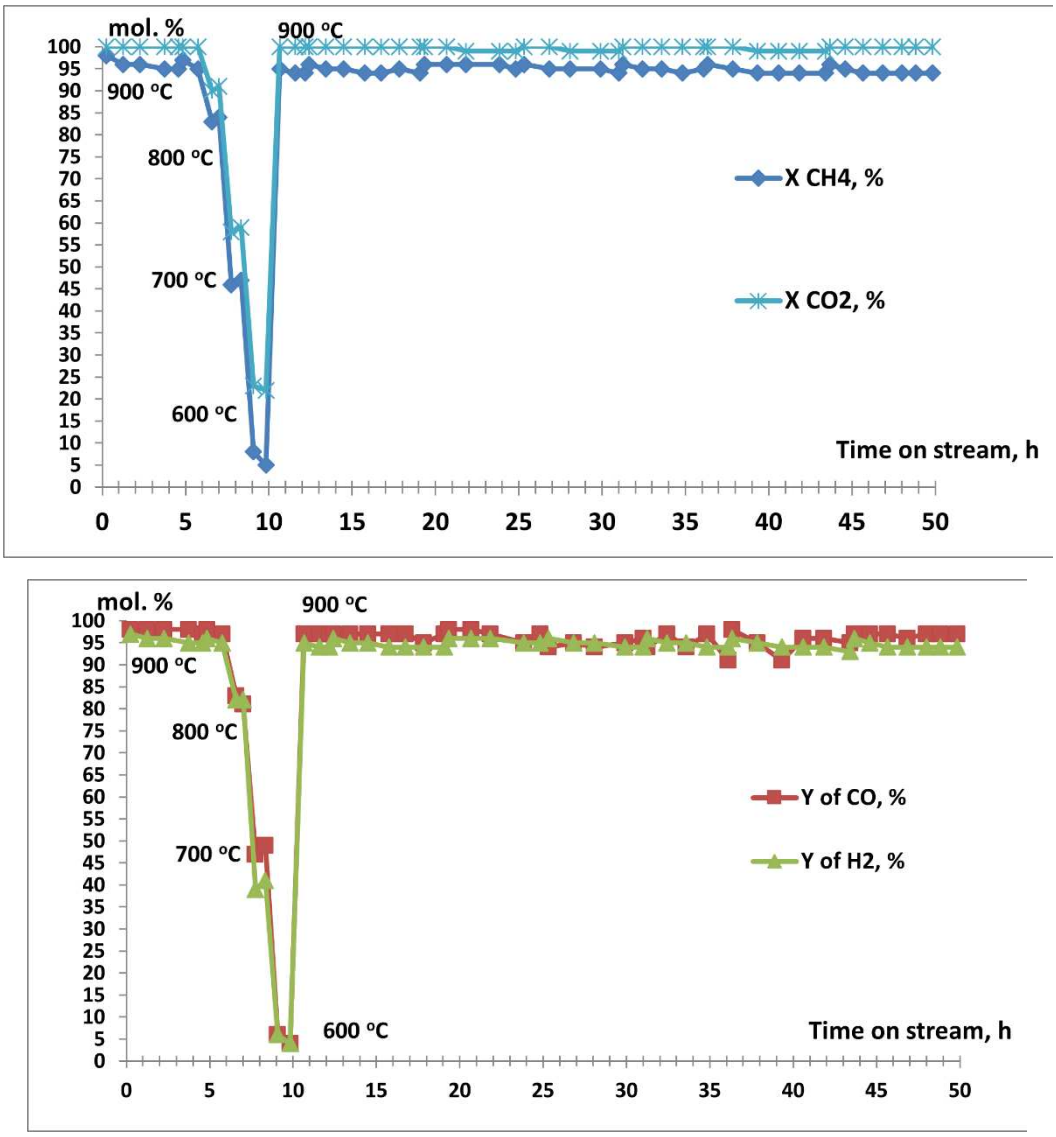

Figure 5. Performance of 5%Co/Sm_2O_3 derived catalyst preheated to 900°C in N_2 flow in DRM process.

According to Figure 6, the catalyst derived from 10%Co/Sm_2O_3 demonstrates similar results in the DRM reaction. After initial heating in nitrogen flow to 900°C, and the subsequent supply of a mixture of CH_4 and CO_2 to the reactor, the CH_4 conversion achieves 97-98% and the CO_2 conversion is as high as 100%. The CO and H_2 yields are 94-95 and 95%, respectively. When temperature was reduced to 800 C, the CH_4 conversion decreased to 84%, the CO_2 conversion decreased to 89-92%, the CO yield decreased to 82-85%, and the H_2 yield decreased to 81-82%. At 700°C a CH_4 conversion of 47%, a CO_2 conversion of 57-61%, a CO yield of 46-47%, and a H_2 yield of 38-40% were observed, while at 600oC almost no DRM occurs. The subsequent increase in temperature to 900°C also restores the activity of the catalyst. When the experiment was continued to 50 h, the high values of CH_4 conversion (94-98%), CO_2 conversion (97-100%), CO yield (95-98%), and H_2 yield (94-98%) were maintained. The higher values of CO_2 conversion and CO yield are also consistent with an insignificant occurrence, along with the DRM reaction (3), of the reverse water gas shift reaction (6), the contribution of which increases with decreasing temperature.

Preprints (www.preprints.org) | NOT PEER-REVIEWED | Posted: 5 July 2023 doi:10.20944/preprints202307.0337.v1

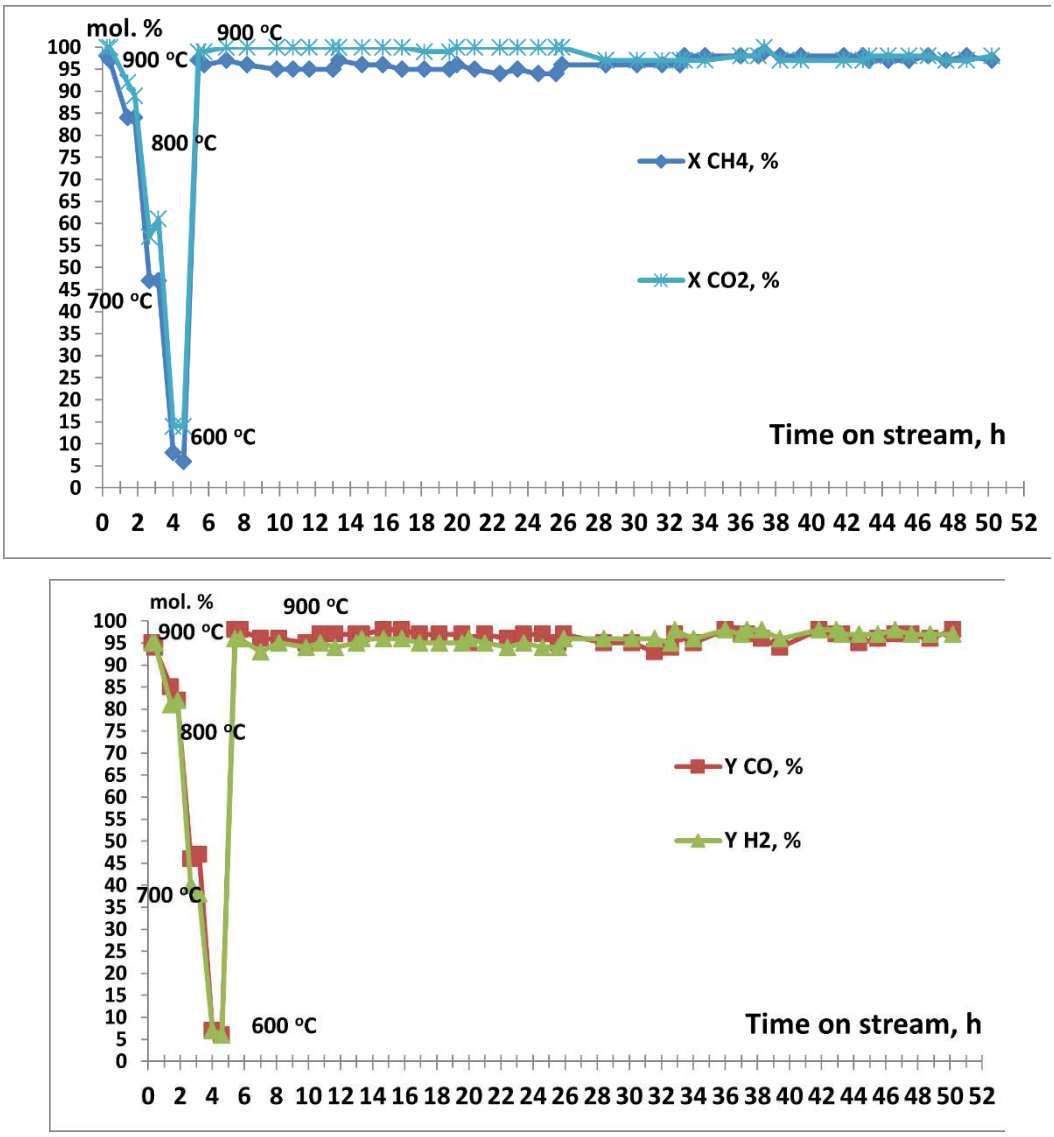

Figure 6. Performance of 10%Co/Sm_2O_3 derived catalyst preheated to 900°C in N_2 flow in DRM.

For comparison, we synthesized and tested a 23%Co/Sm_2O_3 material in the DRM reaction (Figure 7). The same material was previously tested in the DRM reaction after preheating in the reagent stream [35]. According to [35], at 900°C the formed catalyst shows a synthesis gas yield close to quantitative but contains 44.5 wt. % of carbon deposits. Taking into account the data from [35] and the tests of catalysts based on 2%Co/Sm_2O_3, 5%Co/Sm_2O_3, and 10%Co/Sm_2O_3, in the present work, this material was tested in the DRM reaction after preheating to 900°C for an hour in the high-purity nitrogen stream. Figure 7 demonstrates that for 55 h the catalyst formed from 23%Co/Sm_2O_3 retained 95-98% CH_4 conversion, 98-100% CO_2 conversion, 95-98% CO yield, and 94-97% H_2 yield. At the same time, the data in Figure 7 confirm that, along with the DRM reaction (3), an insignificant reverse the water gas shift reaction (6) proceeds.

Preprints (www.preprints.org) | NOT PEER-REVIEWED | Posted: 5 July 2023 doi:10.20944/preprints202307.0337.v1

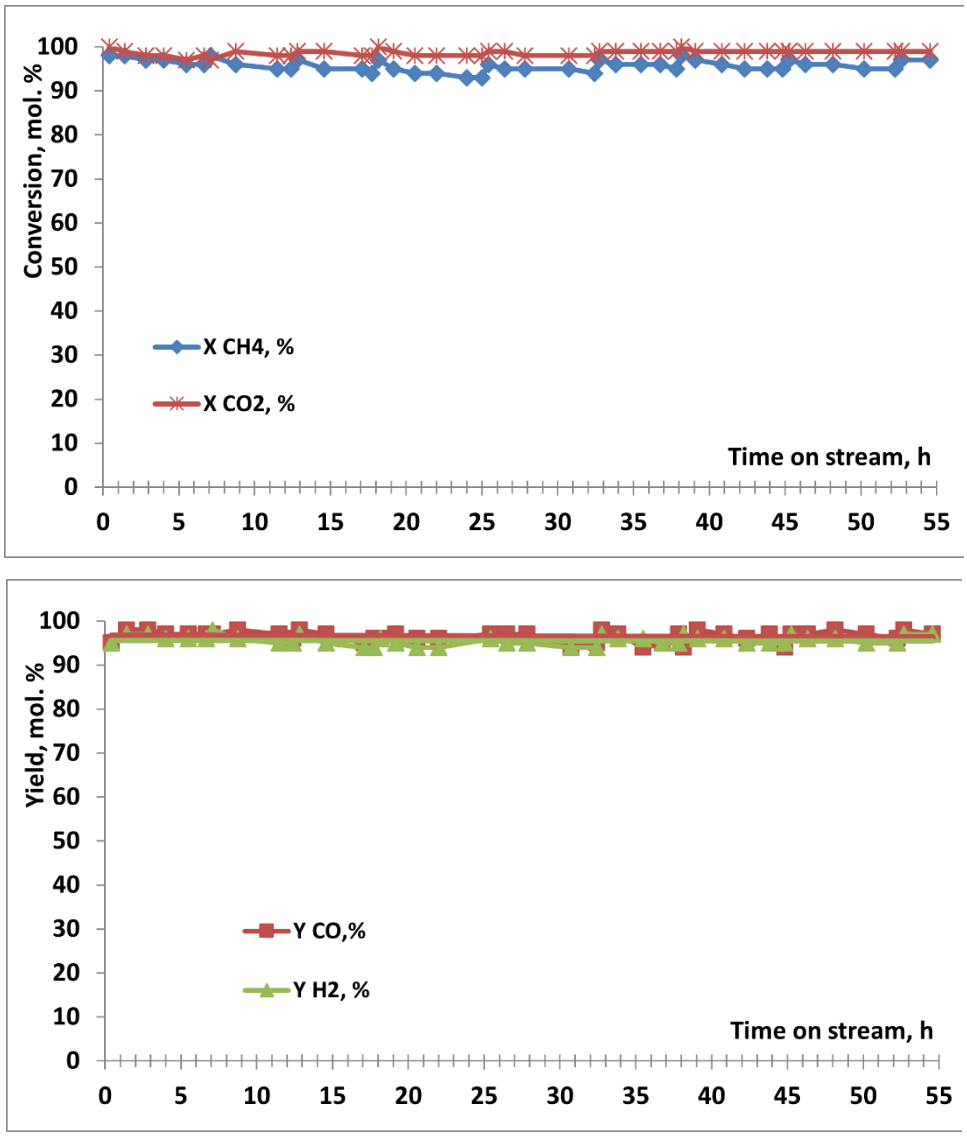

Figure 7. Performance of 23%Co/Sm_2O_3 derived catalyst preheated to 900°C in N_2 flow in DRM process.

The catalysts formed during the DRM process and discharged from the reactor were investigated by XRD, TGA and TEM methods.

The XRD data of the spent catalysts are shown in Figure 8.

The XRD pattern of the spent catalyst derived from 2%Co/Sm_2O_3 (Figure 8a) shows only reflections due to cubic Sm_2O_3 (ICDD 96-101-0590) and rhombic Sm_2O_3 (ICDD 96-153-0725). The absence of reflections due to cobalt and its compounds may be explained by a small number of particles and their small size.

The XRD pattern of the spent catalyst derived from 5%Co/Sm_2O_3 (Figure 8b) exhibits, along with reflections due to cubic Sm_2O_3 (ICDD 96-901-5549) and rhombic Sm_2O_3 (ICDD 96-153-0725), reflections corresponding to metallic cobalt (ICDD 96-901-0969). In this case, the size of cobalt particles could not be correctly estimated according to the Debye-Scherrer formula.

Preprints (www.preprints.org) | NOT PEER-REVIEWED | Posted: 5 July 2023 doi:10.20944/preprints202307.0337.v1

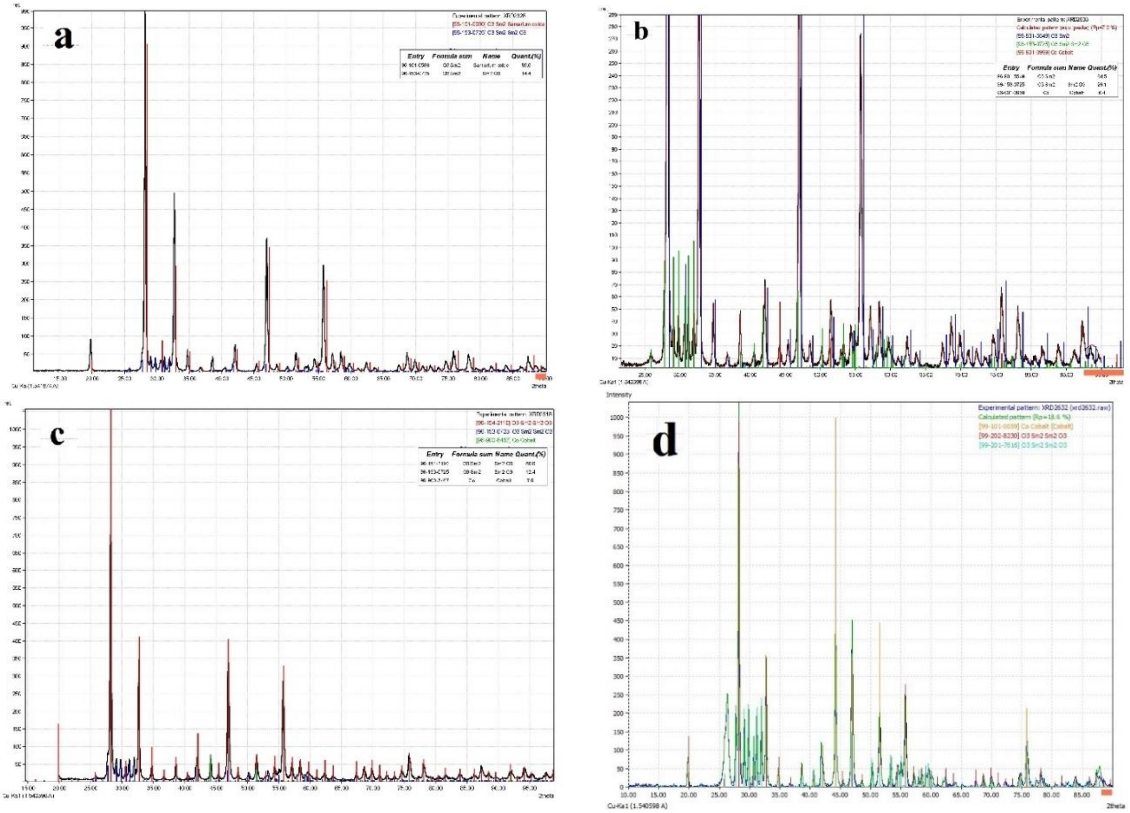

Figure 8. XRD patterns of spent catalysts derived from (**a**) 2%Co/Sm_2O_3, (**b**) 5%Co/Sm_2O_3, (**c**) 10%Co/Sm_2O_3, and (**d**) 23%Co/Sm_2O_3.

The XRD pattern of the spent catalyst derived from 10%Co/Sm_2O_3 (Figure 8c) contains reflections due to cubic Sm_2O_3 (ICDD 96-154-2110), rhombic Sm_2O_3 (ICDD 96-153-0725), and metallic cobalt (ICDD 96-900-8467). In accordance with the Debye-Scherrer formula, the size of cobalt particles is 52 and 56 nm.

The XRD pattern of the spent catalyst derived from 23%Co/Sm_2O_3 (Figure 8d) shows reflections related to cubic Sm_2O_3 (ICDD 99-201-7616), rhombic Sm_2O_3 (ICDD 99-202-8230), and metallic cobalt (ICDD 99-101-0059). In accordance with the Debye-Scherrer formula, the size of cobalt particles is 43 and 48 nm.

Thus, the XRD data (Figure 8) indicate that the true DRM catalysts are Co/Sm_2O_3 composites of metallic cobalt dispersed in samarium oxide, which are derived from 2%Co/Sm_2O_3, 5%Co/Sm_2O_3, 10%Co/Sm_2O_3, and 23%Co/Sm_2O_3. It should be noted that all the formed composites maintain high activity in DRM for at least 50 h.

The TGA data obtained for the spent catalysts are shown in Figures 9a-d.

All the samples are characterized by a slight initial weight loss associated with the removal of adsorbed water and gases upon heating to 300°C. At higher temperatures, marked differences in TGA profiles are observed.

The TGA profile of the spent catalyst derived from 2%Co/Sm_2O_3 (Figure 9a) shows that upon heating from 350 to 450 °C, the weight slightly increases apparently due to the oxidation of metallic cobalt. At 450-650°C the weight decreases by 0.26%, which correlates with the combustion of carbonaceous deposits and the decomposition of carbonates. A slight weight loss at 650-750°C may be attributed to the combustion of carbon, and a subsequent increase in weight can be explained by the resynthesis of cobalt-samarium complex oxides.

Preprints (www.preprints.org) | NOT PEER-REVIEWED | Posted: 5 July 2023 doi:10.20944/preprints202307.0337.v1

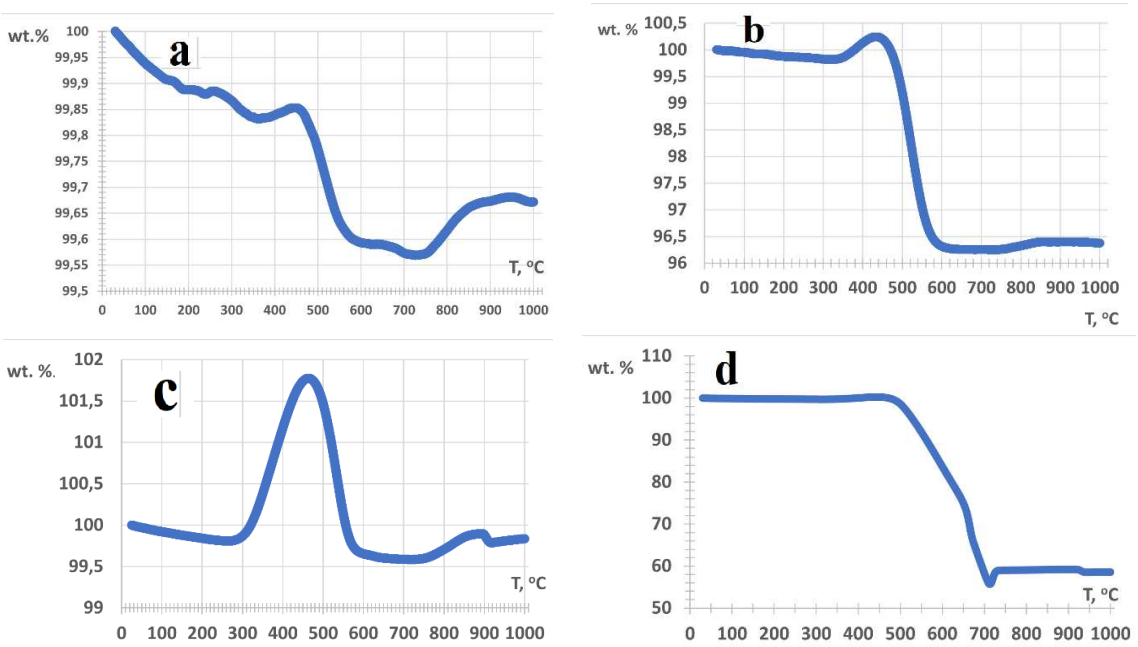

Figure 9. TGA profiles of the spent catalysts derived from (**a**) 2%Co/Sm_2O_3, (**b**) 5%Co/Sm_2O_3, (**c**) 10%Co/Sm_2O_3, and (**d**) 23%Co/Sm_2O_3.

The TGA profile of the spent catalyst derived from 5%Co/Sm_2O_3 (Figure 9b) indicates that upon heating from 320 to 440°C weight increases by 0.42% evidently due to the oxidation of metallic cobalt. At 440-730°C the weight decreases by 4%, in correlation with the combustion of carbonaceous deposits and the decomposition of carbonates. A slight weight loss at 650-750°C may also be associated with the combustion of carbon. A subsequent slight increase in weight is presumably caused by the resynthesis of cobalt-samarium complex oxides.

The TGA profile of the spent catalyst derived from 10%Co/Sm_2O_3 (Figure 9c) shows that upon heating from 260 to 460°C weight increases by 2%, which is apparently related to the oxidation of metallic cobalt. At 460-720°C the weight loss is 2.2%. This is apparently associated with the combustion of carbonaceous deposits and the decomposition of carbonates. Above 720°C, weight increases by 0.31% which is evidently due to the resynthesis of cobalt-samarium complex oxides.

The TGA data on the spent catalyst derived from 23%Co/Sm_2O_3, (Figure 9d) demonstrate that upon heating from 260 to 460°C an increase in weight is as low as 0.54%. This can apparently be explained by oxidation of metallic cobalt. At 460-620°C weight decreases by 20.72%. This is apparently due to the combustion of amorphous carbonaceous deposits and the decomposition of carbonates. Heating from 620 to 720°C resulted in a weight loss of 23.87% probably due to the combustion of graphite-like carbon. Above 720°C, there is a 3.5% increase in weight, which is apparently related to the resynthesis of cobalt-samarium complex oxides.

Thus, the TGA data of all the studied samples indicate the presence of metallic cobalt in the formed composites. The TGA data suggest that the catalyst formed from 2%Co/Sm_2O_3 is almost not subject to carburization. Catalysts based on 5%Co/Sm_2O_3 and 10%Co/Sm_2O_3 are carbonized to a small extent, whereas the catalyst based on 23%Co/Sm_2O_3 undergoes strong carbonization although it does not lose activity in DRM for more than 50 h.

The TGA results are consistent with the SEM data (Figure 10 a-d).

Preprints (www.preprints.org) | NOT PEER-REVIEWED | Posted: 5 July 2023 doi:10.20944/preprints202307.0337.v1

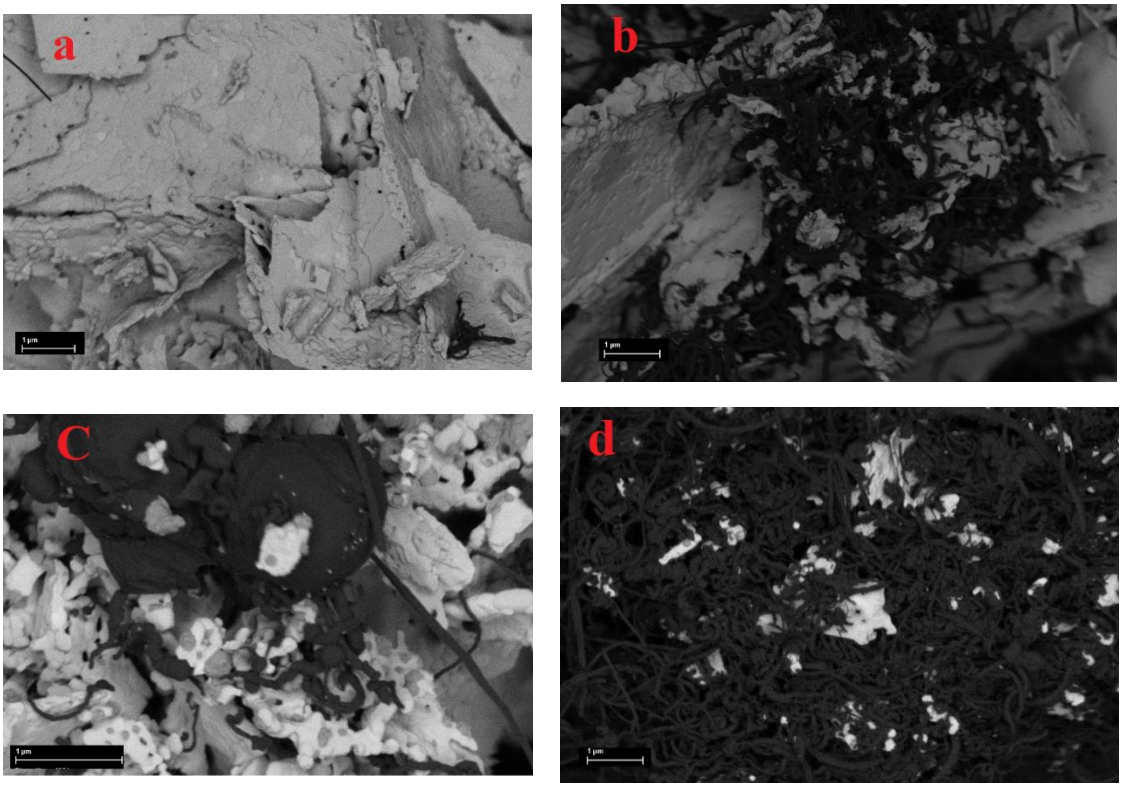

Figure 10. ESB SEM images of spent catalysts derived from (**a**) 2%Co/Sm_2O_3, (**b**) 5%Co/Sm_2O_3, (**c**) 10%Co/Sm_2O_3 (**c**), and (**d**) 23%Co/Sm_2O_3.

The spent catalyst derived from 2%Co/Sm_2O_3 (Figure 10a) contains almost no carbon deposits. The spent catalysts based on 5%Co/Sm_2O_3 (Figure 10b) and 10%Co/Sm_2O_3 (Figure 10c), underwent noticeable carbonization, and the surface of the spent catalyst derived from 23%Co/Sm_2O_3 (Figure 10d) is almost completely covered with carbon deposits.

Spent catalysts with the lowest cobalt content, which were derived from 2%Co/Sm_2O_3 and 5%Co/Sm_2O_3, were additionally investigated by the TEM method. The TEM micrograph of the spent catalyst based on 2%Co/Sm_2O_3 (Figure 11a) demonstrates formation of an insignificant amount of carbon nanotubes. Figure 11b shows that the catalyst contains cobalt particles with a size of about 20 nm.

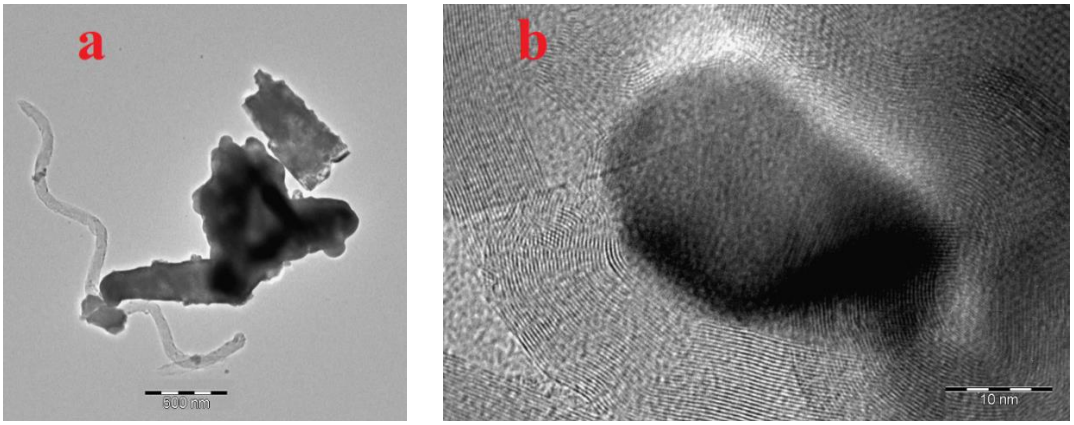

Figure 11. TEM images of spent catalyst derived from 2%Co/Sm_2O_3.

Figure 12 presents the TEM data on the elemental composition and distribution of cobalt and samarium in the spent catalyst derived from 2%Co/Sm_2O_3. It can be seen that cobalt atoms are evenly distributed in samarium oxide.

Preprints (www.preprints.org) | NOT PEER-REVIEWED | Posted: 5 July 2023 doi:10.20944/preprints202307.0337.v1

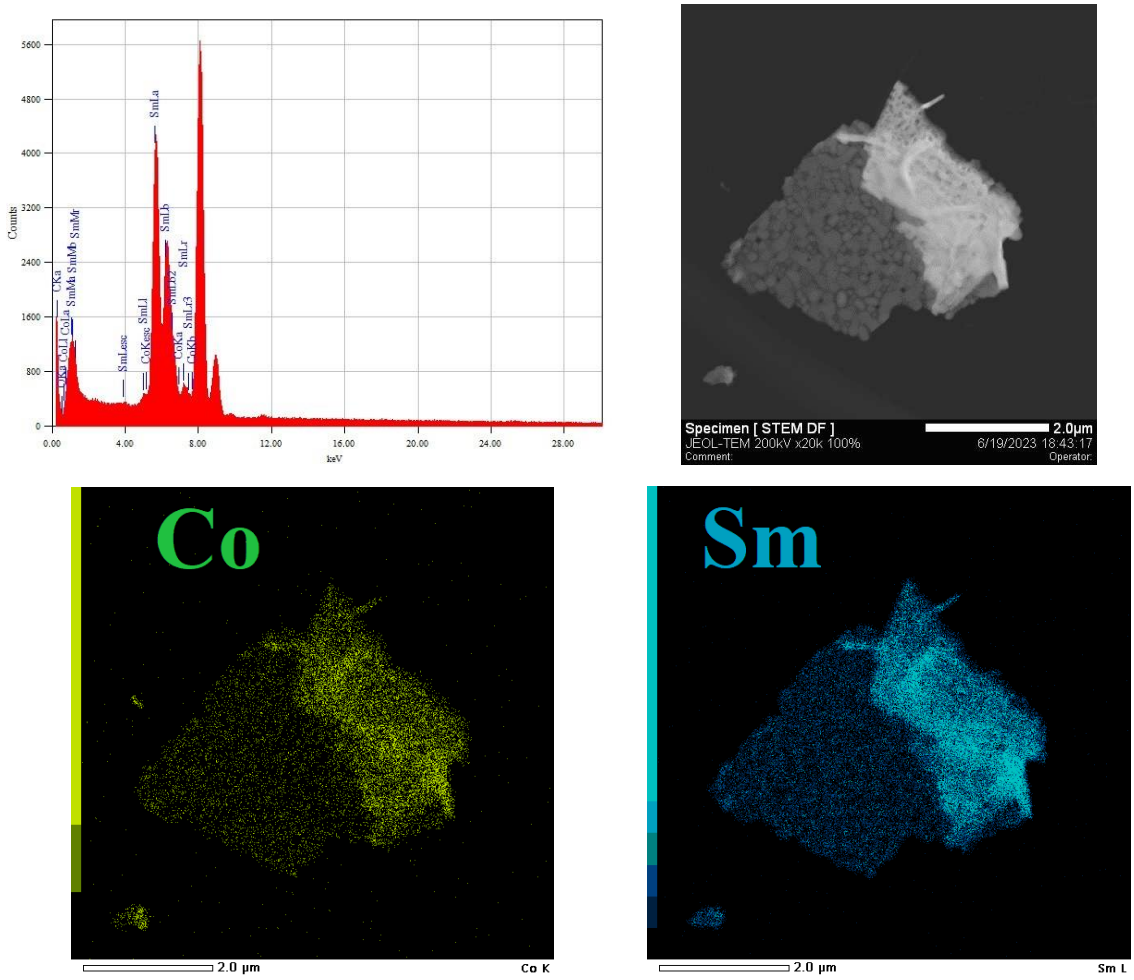

Figure 12. TEM images for the spent catalyst derived from 2%Co/Sm_2O_3: overall elemental spectra, STEM DF image; Co and Sm elemental maps.

For comparison, the spent catalyst derived from 5%Co/Sm_2O_3, which is more prone to carbonization, was also investigated by TEM (Figure 13).

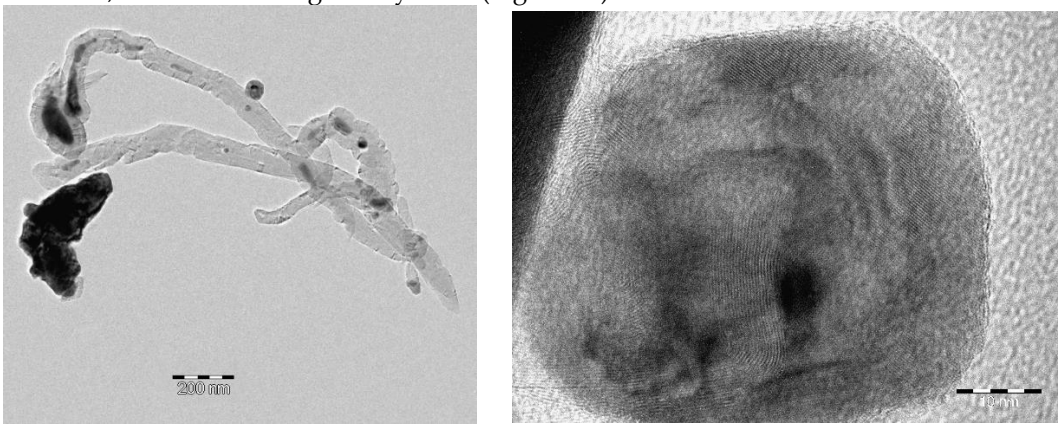

Figure 13. TEM images of spent catalyst derived from 5%Co/Sm_2O_3.

The TEM micrographs shows that the sample contains non-surface-bound carbon nanotubes and cobalt-containing particles up to 50 nm in size. A higher tendency of this sample to coking may be explained by an increase in the size of cobalt-containing particles.

The study of the elemental composition of this material (Figure 14) also showed that the distribution regions of cobalt and samarium atoms in the sample are coincident.

Preprints (www.preprints.org) | NOT PEER-REVIEWED | Posted: 5 July 2023 doi:10.20944/preprints202307.0337.v1

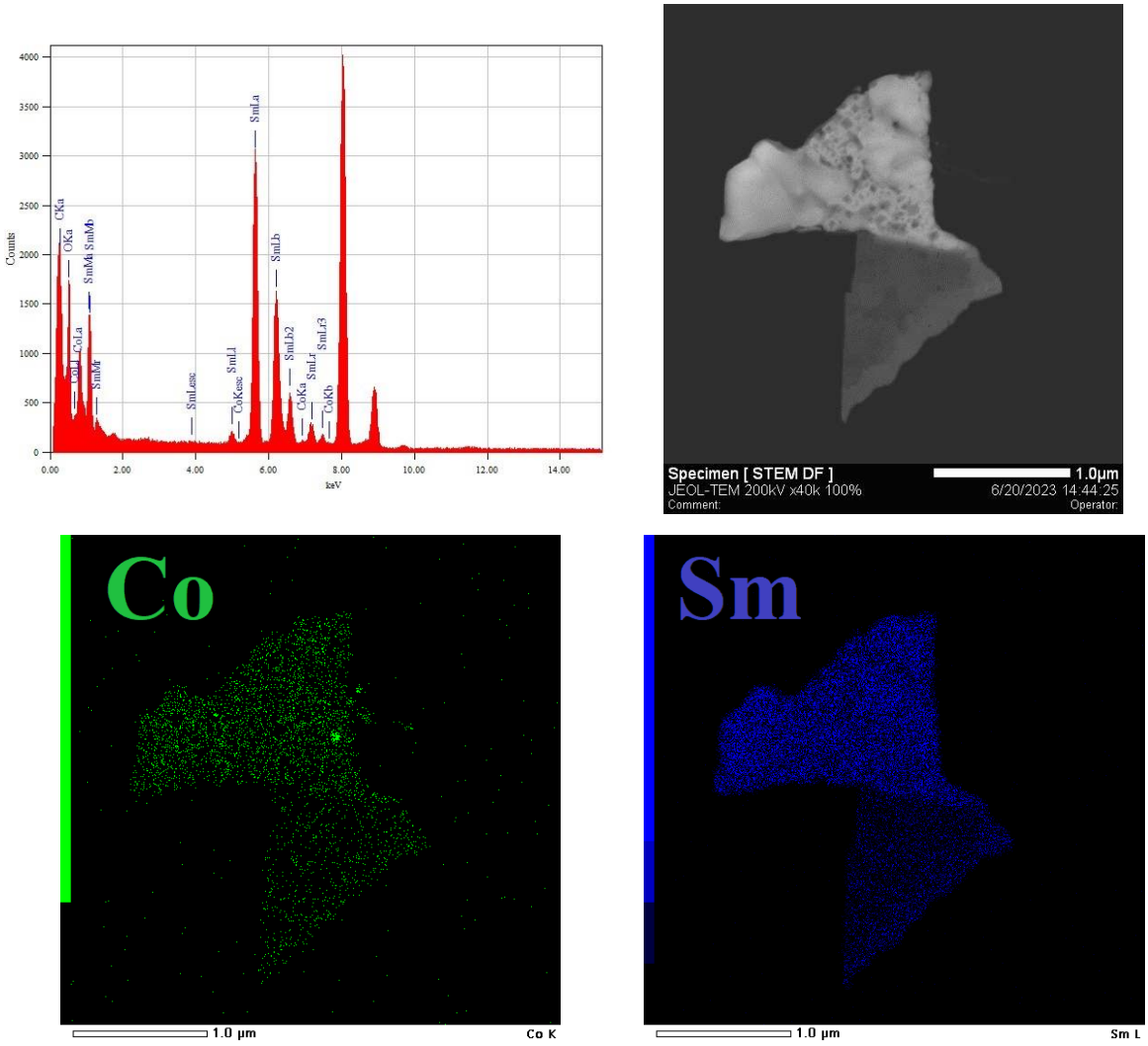

Figure 14. TEM images for the spent catalyst derived from 5%Co/Sm_2O_3: overall elemental spectra, STEM DF image; Co and Sm elemental maps.

Thus, the simple method of synthesizing catalyst precursors, namely, evaporation of aqueous solutions of cobalt and samarium nitrates with subsequent calcination of the resulting material enables one to obtain materials that are precursors of selective and stable catalysts of the DRM reaction. This method is much simpler than most of the known methods used to prepare highly efficient and stable catalysts of this reaction on the basis of cobalt-samarium precursors [7,11,29–31], including single-phase perovskite $SmCoO_3$ [29–31].

An effective way is developed to achieve high synthesis gas yields using the synthesized precatalysts which consists in heating samples in a nitrogen flow to an optimal temperature of 900°C. This DRM procure does not require catalyst pre-reduction by hydrogen or a CH_4/CO_2 mixture. The stable operation of the catalysts lasts for 50 h, and the yields of H_2 and CO close to the thermodynamically predicted limits are achieved. The TGA and SEM data indicate that a high cobalt content in the precatalyst is not required to create a selective, stable, and carbonization resistant DRM catalyst. An increase in the cobalt content in the samples does not affect their stability for 50 h but significantly increases carbonization, which may hinder a longer stable operation of DRM catalysts.

4. Conclusions

The new simple method has been developed for the synthesis of materials that are effective precursors of catalysts for the production of hydrogen and carbon monoxide by the DRM reaction. It is shown that the amount of cobalt introduced into the precatalyst affects its phase composition. For

example, according to XRD data, the 2%Co/Sm_2O_3 sample contains Sm_2O_3 and Sm_2CoO_4 phases. Materials based on 5%Co/Sm_2O_3 and 10%Co/Sm_2O_3 contain $SmCoO_3$ along with Sm_2O_3. The 23%Co/Sm_2O_3 sample containing the same amount of cobalt as $SmCoO_3$ perovskite consists of $SmCoO_3$, Sm_2O_3, and Co_3O_4.

It has been demonstrated that the formation of efficient and stable DRM catalysts based on the synthesized materials does not require their pre-reduction with hydrogen or the initial mixture of reagents. The heating of the synthesized materials up to 900°C in a nitrogen flow and the subsequent supply of the equimolar CH_4/CO_2 mixture allow one to *in situ* obtain a selective and stable DRM catalyst operating for at least 50 h.

It has been shown that the cobalt content in the pre-catalyst significantly affects the carbonization resistance of the formed DRM catalyst. For example, the catalyst derived from 2%Co/Sm_2O_3 is not subject to carbonization when tested in DRM for 50 h. The catalysts based on 5%Co/Sm_2O_3 and 10%Co/Sm_2O_3 undergo noticeable carbonization, which, however, does not worsen the results of DRM for 50 h. The 23%Co/Sm_2O_3 derived catalyst containing the same amount of cobalt as perovskite $SmCoO_3$ maintains stability in the DRM reaction for 50 h but forms a significant amount of carbon, which likely affects its stability during long-term operation. This implies that a cobalt content of 2 wt. % is optimal for obtaining the stable cobalt-samarium DRM catalyst, provided its preheating to 900°C in a nitrogen flow followed by the supply of reagents. The stability of this catalyst is associated with the formation of sintering-resistant cobalt metal particles with a size of about 20 nm. Similar observations were made in the study of DRM using supported nickel and nickel-cobalt catalysts containing these metals in an amount of no more than 2 wt. % [5,40].

In general, the catalyst formed from the 2%Co/Sm_2O_3 material is promising for practical use, since it is almost not subject to carbonization and sintering of cobalt particles and demonstrates consistently high yields of H_2 and CO. Its application in the DRM reaction makes it possible to efficiently utilize two greenhouse gases, methane and carbon dioxide, which is of great ecological importance. In addition, it can potentially be used to produce "green" hydrogen by the conversion of renewable raw material--biogas.

6. Patents

Russian Patent Application **RU 2023 113 594 A** (25.05.2023).

Author Contributions: Conceptualization, A.G.D. and A.S.L.; methodology, A.G.D. and A.S.L.; investigation, A.S.L, V.A.A., A.A.S., K.A.C. and G.A.S.; data curation, A.S.L., V.A.A. and M.A.B.; writing—original draft preparation, A.S.L.; writing—review and editing, A.S.L. and A.G.D.; supervision, A.G.D. and A.S.L.C.; funding acquisition, A.G.D. All authors have read and agreed to the published version of the manuscript.

Funding: This research was funded by Russian Science Foundation, grant number 23-13-00098. TGA, H2-TPR and SEM experiments were carried out within the state funding of TIPS RAS. SEM images were obtained at the IGIC RAS Joint Research Center for Physical Methods of Research.

Data Availability Statement: Russian Science Foundation, https://rscf.ru/project/

Conflicts of Interest: The authors declare no conflict of interest.

References

1. Jang, W.-J.; Shim, J.-O.; Kim, H.-M.; Yoo, S.-Y.; Roh, H.-S. A review on dry reforming of methane in aspect of catalytic properties. *Catal. Today* **2019**, *324*, 15-26. https://doi.org/10.1016/j.cattod.2018.07.032.
2. Su, B.; Wang, Y.; Xu, Z.; Han, W.; Jin, H.; Wang, H. Novel ways for hydrogen production based on methane steam and dry reforming integrated with carbon capture. *Energy Conversion and Management* **2022**, *270*, 116199. https://doi.org/10.1016/j.enconman.2022.116199.
3. Singh, R.; Dhir, A.; Mohapatra, S.K.; Mahla, S.K. Dry reforming of methane using various catalysts in the process: review. *Biomass Conv. Bioref.* **2020,** *10*, 567–587. https://doi.org/10.1007/s13399-019-00417-1
4. Holmen, A. Direct Conversion of Methane to Fuels and Chemicals. *Catal. Today* **2009**, *142*, 2–8. http://dx.doi.org/10.1016/j.cattod.2009.01.004.

5. Moiseev, I.I.; Loktev, A.S.; Shlyakhtin, O.A.; Mazo, G.N.; Dedov, A.G. New approaches to the design of nickel, cobalt, and nickel–cobalt catalysts for partial oxidation and dry reforming of methane to synthesis gas. *Petrol. Chem.* **2019**, *59*, Suppl. 1, S1-S27. https://doi.org/10.1134/S0965544119130115
6. Chen, L.; Qi, Z.; Zhang, S.; Su, J.; Somorjai, G.A. Catalytic Hydrogen Production from Methane: A Review on Recent Progress and Prospect. *Catalysts* **2020**, *10*, 858-876. https://doi.org/10.3390/catal10080858
7. Elbadawi, A.H.; Ge, L.; Li, Z.; Liu, S.; Wang, S.; Zhu, Z. Catalytic partial oxidation of methane to syngas: review of perovskite catalysts and membrane reactors. *Catal. Rev.* **2021**, *63*, 1–67. https://doi.org/10.1080/01614940.2020.1743420.
8. Al-Sayari, S.A. Recent Developments in the Partial Oxidation of Methane to Syngas. *Open Catalysis J.* **2013**, *6*, 17-28. http://dx.doi.org/10.2174/1876214X20130729001
9. Alhassan, M.; Jalil, A.A.; Nabgan, W.; Hamid, M.Y.S.; Bahari, M.B.; Ikram, M. Bibliometric studies and impediments to valorization of dry reforming of methane for hydrogen pro-duction. *Fuel* **2022**, *328*, 125240. https://doi.org/10.1016/j.fuel.2022.125240.
10. Kumar, R.; Kumar, A.; Pal, A. Overview of hydrogen production from biogas reforming: Technological advancement. *Intern. J. of Hydrogen Energy* **2022,** *47*, P. 34831-34855. https://doi.org/10.1016/j.ijhydene.2022.08.059
11. Bhattar, S.; Abedin, Md.A.; Kanitkar, S.; Spivey, J.J. A review on dry reforming of methane over perovskite derived catalysts. *Catal. Today* **2021**, *365*, 2–23. https://doi.org/10.1016/j.cattod.2020.10.041.
12. The, L.P.; Setiabudi, H.D.; Timmiati, S.N.; Aziz, M.A.A.; Annuar, N.H.R.; Ruslan, N.N. Recent progress in ceria-based catalysts for the dry reforming of methane: A review. *Chem. Engineering Sci.* **2021**, *242*, 116606. https://doi.org/10.1016/j.ces.2021.116606.
13. Yentekakis, I.V.; Panagiotopoulou, P.; Artemakis, G. A review of recent efforts to promote dry reforming of methane (DRM) to syngas production via bimetallic catalyst formulations. *Appl. Catal. B: Environmental* **2021**, *296*, 120210. https://doi.org/10.1016/j.apcatb.2021.120210.
14. Wang, C.; Wang, Y.; Chen, M.; Liang, D.; Yang, Z.; Cheng, W.; Tang, Z.; Wang, J.; Zhang, H. Recent advances during CH_4 dry reforming for syngas production: A mini review. *Intern. J. of Hydrogen Energy*, **2021**, *46*, 5852–5874. https://doi.org/10.1016/j.ijhydene.2020.10.240.
15. le Saché, E.; Reina, T.R. Analysis of dry reforming as direct route for gas phase CO_2 conversion. The past, the present and future of catalytic DRM technologies. *Progr. in Energy and Combustion Sci.* **2022,** *89*, 100970. https://doi.org/10.1016/j.pecs.2021.100970.
16. Hambali, H.U.; Jalil, A.A.; Abdulrasheed, A.A.; Siang, T.J.; Gambo, Y.; Umar, A.A. Zeolite and clay based catalysts for CO_2 reforming of methane to syngas: A review. *Intern. J. of Hydrogen Energy* **2022**, *47*, 30759–30787. https://doi.org/10.1016/j.ijhydene.2021.12.214.
17. Baharudin, L.; Rahmat, N.; Othman, N.H.; Shah, N.; Syed-Hassan, S.S.A. Formation, control, and elimination of carbon on Ni-based catalyst during CO_2 and CH_4 conversion via dry reforming process: A review. *J. of CO_2 Utilization* **2022**, *61*, 102050. https://doi.org/10.1016/j.jcou.2022.102050.
18. Mortensen, P.M.; Dybkjær, I. Industrial scale experience on steam reforming of CO_2-rich gas. *Appl. Catal. A: General* **2015**, *495*, 141–151. https://doi.org/10.1016/j.apcata.2015.02.022.
19. Teuner, S.C.; Neumann, P.; Von Linde, F. The Calcor standard and Calcor economy processes. *OIL GAS European Magazine* **2001**, *№ 3*, 44–46. https://www.caloric.com/wp-content/uploads/2016/11/Caloric-Downloads-Calcor.pdf
20. Usman, M.; Wan Daud, W.M.A.; Abbas, H.F. Dry reforming of methane: Influence of process parameters. A review. *Renewable and Sustainable Energy Rev.* **2015**, *45*, 710–744. https://doi.org/10.1016/j.rser.2015.02.026.
21. Schulz, L.A.; Kahle, L.C.S.; Delgado, K.H.; Schunk, S.A.; Jentys, A.; Deutschmann, O.; Lercher, J.A. On the coke deposition in dry reforming of methane at elevated pressures. *Appl. Catal. A: General* **2015**, *504*, 599–607. https://doi.org/10.1016/j.apcata.2015.03.002.
22. Jang, W.-J.; Jeong, D.-W.; Shim, J.-O.; Kim, H.-M.; Roh, H.-S.; Son, I.H.; Lee, S.J. Combined steam and carbon dioxide reforming of methane and side reactions: Thermodynamic equilibrium analysis and experimental application. *Appl. Energy* **2016**, *173*, 80–91. https://doi.org/10.1016/j.apenergy.2016.04.006.
23. Yusuf, M.; Farooqi, A.S.; Keong, L.K.; Hellgardt, K.; Abdullah, B. Contemporary trends in composite Ni-based catalysts for CO_2 reforming of methane. *Chem. Engineering Science* **2021**, *229*, 116072. https://doi.org/10.1016/j.ces.2020.116072.,
24. Jafarbegloo, M.; Tarlani, A.; Wahid Mesbah, A.; Sahebdelfar, S. Thermodynamic analysis of carbon dioxide reforming of methane and its practical relevance. *Intern. J. of Hydrogen Energy* **2015**, *40*, 2445-2451. https://doi.org/10.1016/j.ijhydene.2014.12.103.,
25. Khoshtinat Nikoo, M.; Amin, N.A.S. Thermodynamic analysis of carbon dioxide reforming of methane in view of solid carbon formation. *Fuel Process. Technol.* **2011**, *92*, 678-691. https://doi.org/10.1016/j.fuproc.2010.11.027.
26. Aziz, M.A.A.; Setiabudi, H.D.; Teh, L.P.; Annuar, N.H.R.; Jalil, A.A. A review of heterogeneous catalysts for syngas production via dry reforming. *J. of the Taiwan Institute of Chem. Engineers* **2019**, *101*, 139-158. https://doi.org/10.1016/j.jtice.2019.04.047.

27. Choudhary, V.R.; Mondal, K.C.; Mamman, A.S.; Joshi, U.A. Carbon-free dry reforming of methane to syngas over $NdCoO_3$ perovskite-type mixed metal oxide catalyst. *Catal. Lett.* **2005**, *100*, 271-276. https://doi.org/10.1007/s10562-004-3467-0
28. Royer, S.; Duprez, D.; Can, F.; Courtois, X.; Batiot-Dupeyrat, C.; Laassiri, S.; Alamdari, H. Perovskites as Substitutes of Noble Metals for Heterogeneous Catalysis: Dream or Reality. *Chem. Rev.* **2014**, *114*, 10292-10368. https://doi.org/10.1021/cr500032a
29. Gavrikov, A.V.; Loktev, A.S.; Ilyukhin, A.B.; Mukhin, I.E.; Bykov, M.A.; Maslakov, K.I.; Vorobei, A.M.; Parenago, O.O.; Sadovnikov, A.A.; Dedov, A.G. Supercritical Fluid Assisted Modification combined with the Resynthesis of $SmCoO_3$ as Effective Tool to Enhance Long-term Performance of $SmCoO_3$-derived Catalysts for Dry Reforming of Methane to Syngas. *Dalton Trans.* **2022**, *51*, 18446–18461. https://doi.org/10.1039/D2DT03026H
30. Gavrikov, A.V.; Ilyukhin, A.B.; Belova, E.V.; Yapryntsev, A.D.; Dobrokhotova, Z.V.; Khrushcheva, A.V.; Efimov, N.N. Rapid preparation of $SmCoO_3$ perovskite via uncommon though efficient precursors: Composition matters! *Ceram. Int.* **2020**, *46*, 13014–13024. https://doi.org/10.1016/j.ceramint.2020.02.071.
31. Osazuwa, O.U.; Cheng, C.K. Catalytic conversion of methane and carbon dioxide (greenhouse gases. into syngas over samarium-cobalt-trioxides perovskite catalyst. *J. of Cleaner Production* **2017**, *148*, 202–211. https://doi.org/10.1016/j.jclepro.2017.01.177
32. Salaev, M.A.; Liotta, L.F.; Vodyankina, O.V. Lanthanoid-containing Ni-based catalysts for dry reforming of methane: A review. *Int. J. of Hydrogen Energy* **2022**, *47*, 4489-4535. https://doi.org/10.1016/j.ijhydene.2021.11.086.
33. de Lira Lima, D.C.; Lemos, I.P.; Gomes, Rodrigues, R.S.; L.M.T.S.; Fréty, R.T.; Resini, C.; Junior, R.B.S.; Brandão, S.T. Study of $LaNi_{1-x}Co_xO_3$ Perovskites-Type Oxides Either Pure or Mixed with SiO_2 as Catalytic Precursors Applied in CH_4 Dry-Reforming. *Catal Lett.* **2023,** *153*, 2137–2148. https://doi.org/10.1007/s10562-022-04127-8
34. Dedov, A.G.; Loktev, A.S.; Ivanov, V.K.; Bykov, M.A.; Mukhin, I.E.; Lidzhiev, M.M.; Rogaleva, E.V.; Moiseev, I.I. Selective oxidation of methane to synthesis gas: Cobalt- and nickel-based catalysts. *Doklady Phys. Chemistry* **2015**, *461*, 73-79. https://doi.org/10.1134/S0012501615040028
35. Loktev, A.S.; Mukhin, I.E.; Bykov, M.A.; Sadovnikov, A.A.; Osipov, A.K.; Dedov A.G. Novel high-performance catalysts for partial oxidation and dry reforming of methane to synthesis gas. *Petrol. Chemistry* **2022**, *62*, 526–543. https://doi.org/10.1134/S0965544122020207.
36. Loktev, A.S.; Arkhipova, V.A.; Bykov, M.A.; Sadovnikov, A.A.; Dedov, A.G. Cobalt–Samarium Oxide Composite as a Novel High-Performance Catalyst for Partial Oxidation and Dry Reforming of Methane into Synthesis Gas. *Petrol. Chemistry* **2023**, Open access publication: https://doi.org/10.1134/S0965544123010048
37. Rietveld, H.M. A profile refinement method for nuclear and magnetic structures. *J. of Appl. Crystallography* **1969**, *2*, 65—71. doi:10.1107/S0021889869006558
38. Olusola, J.O.; Sudip, M. Temperature programme reduction (TPR) studies of cobalt phases in γ-alumina supported cobalt catalysts. *J. of Petrol. Technol. and Alternative Fuels* **2016**, *7*, 1-12. DOI: 10.5897/JPTAF2015.0122.
39. Ma, F.; Chen, Y.; Lou, H. Characterization of perovskite-type oxide catalysts $RECoO_3$ by TPR. *React. Kinet. Catal. Lett.* **1986**, *31*, 47-53.
40. Dedov, A.G.; Loktev, A.S.; Mukhin, I.E.; Baranchikov, A.E.; Ivanov, V.K.; Bykov, M.A.; Solodova, E.V.; Moiseev, I.I. Effect of the Support Nature on Stability of Nickel and Nickel–Cobalt Catalysts for Partial Oxidation and Dry Reforming of Methane to Synthesis Gas. *Petrol. Chemistry* **2019**, *59*, 385–393. DOI: 10.1134/S0965544119040042